Journal of Soft Computing Exploration
Homepage: htttps://shmpublisher.com/index.php/joscex
p-ISSN: 2746-7686
e-ISSN: 2746-0991

.

Tuberculosis classification on chest x-ray images using DenseNet-169 and convolutional block attention module

Muhammad Agil Izzulhaq[1], Endang Sugiharti[2]
[1,2]Department of Computer Science, Universitas Negeri Semarang, Indonesia

Article Info

Article history:

Received March 12, 2026
Revised March 18, 2026
Accepted March 19, 2026

Keywords:

Tuberculosis
Chest x-ray
DenseNet-169
Convolutional block attention module
Deep learning

ABSTRACT

Tuberculosis remains a major global health challenge, and the manual interpretation of chest X-rays is often limited by the subjectivity and shortage of radiology experts. While deep learning approaches like DenseNet have shown promise in medical imaging, the integration of attention mechanisms such as the Convolutional Block Attention Module (CBAM) for tuberculosis detection has been less explored. This study aimed to develop a Convolutional Neural Network (CNN) model utilizing DenseNet-169 combined with CBAM to accurately classify chest X-ray images into normal and tuberculosis classes. A dataset of 7,000 chest X-ray images was preprocessed and partitioned into training, validation, and testing sets. DenseNet-169 served as the backbone architecture, while CBAM was applied to emphasize crucial spatial and channel features. Evaluated across standard metrics, the proposed model achieved an accuracy of 99.43%, a precision of 99.72%, a recall of 99.14%, and an F1-score of 99.43%, successfully outperforming the baseline DenseNet-169 model without CBAM. Ultimately, the integration of CBAM with DenseNet-169 demonstrates remarkable potential in improving tuberculosis detection, confirming that attention mechanisms can substantially enhance deep learning performance in medical imaging.

Corresponding Author:

Muhammad Agil Izzulhaq,
Department of Computer Science, Faculty of Mathematics and Natural Sciences,
Universitas Negeri Semarang,
Sekaran, Gunungpati, Semarang, Central Java 50229, Indonesia.
Email: agilizzulhaq@students.unnes.ac.id
https://doi.org/10.52465/joscex.v7i1.14

1. INTRODUCTION

Technological advancements have significantly transformed human life, including the healthcare sector [1]. Innovations in digital systems and artificial intelligence have reshaped medical services to become more efficient and integrated [2]. These technologies facilitate faster and more accurate patient data management, service delivery, and medical research. A rapidly expanding area of application lies in the use of intelligent technologies to aid diagnostic procedures, with a particular emphasis on medical imaging methods such as chest X-rays and CT scans [3]. These systems can automatically detect potential disease markers by integrating pattern recognition techniques and visual classification. This not only enhances the accuracy of diagnoses but also shortens the time required for image interpretation and ensures greater consistency in results. As a result, such innovations support earlier medical intervention, improve patient outcomes, and strengthen clinical

decision-making processes [4]. Among the diseases most widely studied in image-based detection systems is tuberculosis.

As one of the most ancient diseases affecting humans, tuberculosis continues to rank among the foremost causes of death across the world [5]. The causative agent is the intracellular pathogen Mycobacterium tuberculosis, which preferentially invades macrophages [6]. Transmission generally occurs through airborne droplets released when infected individuals cough, sneeze, or spit [7]. Active tuberculosis can spread beyond the lungs to other organs through the bloodstream, airways, or lymphatic system [8]. Infections may become active when the immune system is weakened [9]. Despite being preventable and treatable, tuberculosis remains a critical concern for global public health. According to the Global Tuberculosis Report 2024 released by the World Health Organization [10], tuberculosis has reclaimed its position as the foremost cause of death from infectious diseases, overtaking COVID-19. In 2023, 8.2 million new cases and approximately 1.25 million deaths were reported, with a global total of 10.8 million cases and an incidence rate of 134 per 100,000 individuals. Most cases were concentrated in five countries: India, Indonesia, China, the Philippines, and Pakistan. These figures underline the urgent need for more accurate and efficient methods to identify cases at an early stage. Rapid and precise detection is crucial to reducing transmission, improving treatment effectiveness, and lowering the risk of drug resistance [11]. One of the most promising approaches to achieving this is the application of Convolutional Neural Network (CNN)-based methods for the automatic classification of tuberculosis through medical image analysis.

Convolutional Neural Network (CNN) represents one of the most prevalent deep learning methods in image analysis, applied across numerous computer vision tasks and capable of achieving human-level performance by learning from experience [12]. CNN employs convolutional kernels to capture patterns directly from raw data and progressively learn feature representations from extensive datasets. This capability enables CNN to generalize better than traditional image classification methods that rely on manually crafted features [13]. As a result, CNN has become a critical tool in medical imaging, particularly for the automated interpretation of chest X-rays, CT scans, and MRI scans, which are essential for detecting abnormalities and disease markers. Unlike traditional data processing methods, deep learning models like CNN can autonomously identify and learn important features without human intervention [14]. Consequently, CNN are increasingly central to disease diagnosis and the development of technology-driven classification systems, including those designed for detecting tuberculosis.

Recent research has demonstrated the effectiveness of CNN in classifying tuberculosis from medical images, marking significant advancements in applying deep learning in this area. For example, using chest X-ray data from the Shenzhen and Montgomery datasets, Mizan et al. (2020) [15] conducted a comparative study of four pretrained CNN architectures, DenseNet-169, MobileNet, Xception, and Inception-V3. By applying data augmentation and utilizing a comprehensive set of evaluation metrics, DenseNet-169 achieved the highest accuracy, reaching 91.6%. In another study, Y. Liu et al. (2020) [16] introduced CBAM within a ResNet framework to improve tuberculosis detection from chest X-rays. Using a two-stage training strategy (W2F) in conjunction with SGD-GC optimization, the CBAM-enhanced model attained accuracies of 91.1% on the Shenzhen dataset and 86.4% on the Montgomery dataset, surpassing the baseline ResNet, which achieved accuracies of 90.6% and 82.1%, respectively. These studies highlight that integrating CNN models with attention mechanisms can lead to better performance than conventional single-model approaches.

Building on previous research findings, this study presents a model for classifying tuberculosis in chest X-ray images by integrating DenseNet-169 with the Convolutional Block Attention Module (CBAM). DenseNet-169 is highly effective at extracting deep feature representations, while CBAM enhances the model's focus by emphasizing the most informative spatial and channel-wise details. Combining these components is expected to improve tuberculosis classification's accuracy and robustness, providing advantages over traditional CNN-based approaches.

2. METHOD

The research procedure begins with a literature review aimed at establishing a solid understanding of Convolutional Neural Networks (CNNs), the DenseNet-169 architecture, and the role of the Convolutional Block Attention Module (CBAM) in classifying tuberculosis using Chest X-Ray (CXR) images. Once the theoretical foundation is laid, data is collected using a publicly available dataset widely adopted in related studies and recognized for its reliability [17]. Following data collection, the dataset is explored to examine its overall characteristics, including the number of images in each category, image quality, and sample visualizations from both classes. This ensures that the dataset is both relevant and representative. The dataset

is then divided into training, validation, and testing subsets to ensure objective model training and evaluation. Subsequently, preprocessing steps are conducted, including pixel value normalization and image resizing, to meet the input requirements of DenseNet-169. The prepared dataset is used for model development, with DenseNet-169 serving as the baseline architecture and CBAM incorporated into its dense blocks to enhance focus on critical image features. Model performance is evaluated using standard metrics such as accuracy, precision, recall, and F1-score, which collectively assess the effectiveness of CBAM in improving classification performance. Based on the evaluation outcomes, a system design is implemented by deploying the model in a web-based application to facilitate practical use in CXR image classification. Finally, the evaluation results are analyzed to determine the impact of integrating CBAM into tuberculosis classification performance. The workflow applied in this research is depicted in Figure 1.

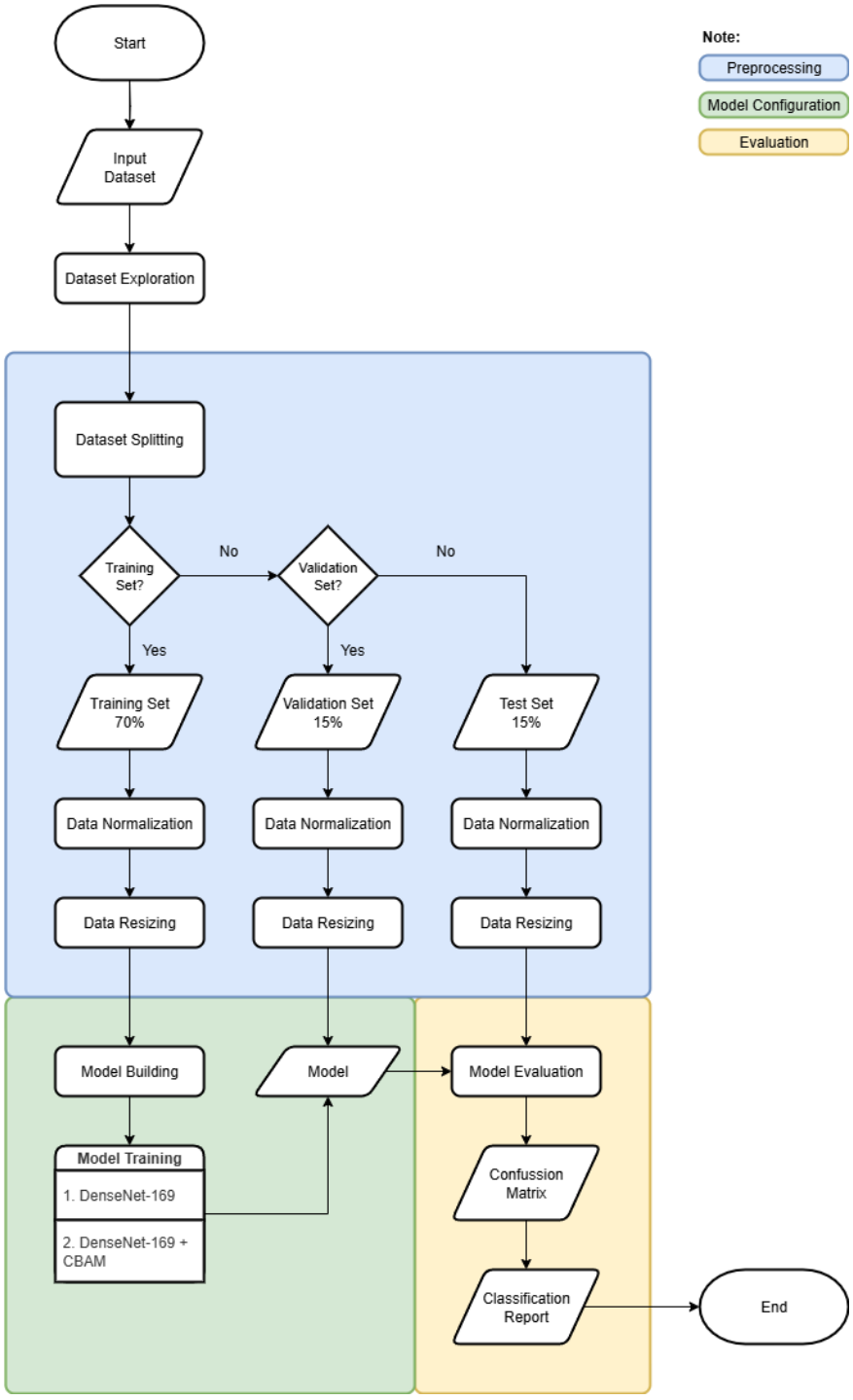

Figure 1. Research methodology

Data Exploration

In the dataset exploration stage, several initial steps were carried out to ensure the quality and suitability of the data before proceeding to model training. The dataset utilized in this study was obtained from a comprehensive database compiling four publicly accessible sources which are the National Library of Medicine (NLM), the Belarus dataset, the NIAID TB dataset, and the RSNA pneumonia detection challenge dataset [17]. In total, the dataset consists of 7,000 chest X-ray images. The number of images in each label was checked to ensure a perfectly balanced distribution, comprising exactly 3,500 normal chest X-ray images and 3,500 tuberculosis-infected images [18]. Following this, an inspection was conducted to identify any damaged or corrupt files that could interfere with the training process, the results of which are illustrated in Figure 2. Specifically, Figure 2(b) presents the image condition distribution, indicating that 100% of the dataset is classified as 'valid.' This confirms that there are no corrupt images, ensuring optimal data integrity for reliable model training. Additionally, sample images from each class were reviewed as visual representations to understand the general characteristics of each category better, providing an early insight into the visual differences between normal and tuberculosis-indicated images, shown in Figure 3.

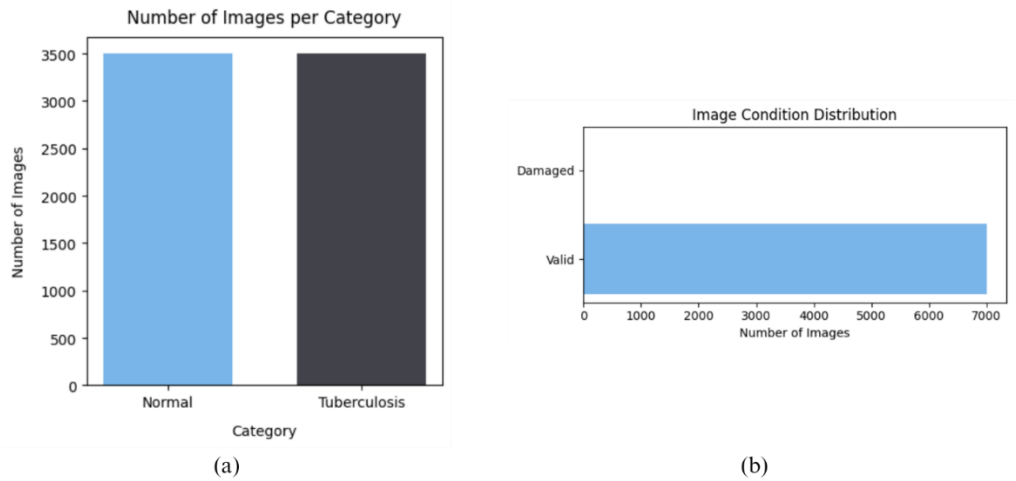

Figure 2. Data distribution based on (a) Number of images per category; (b) Image condition

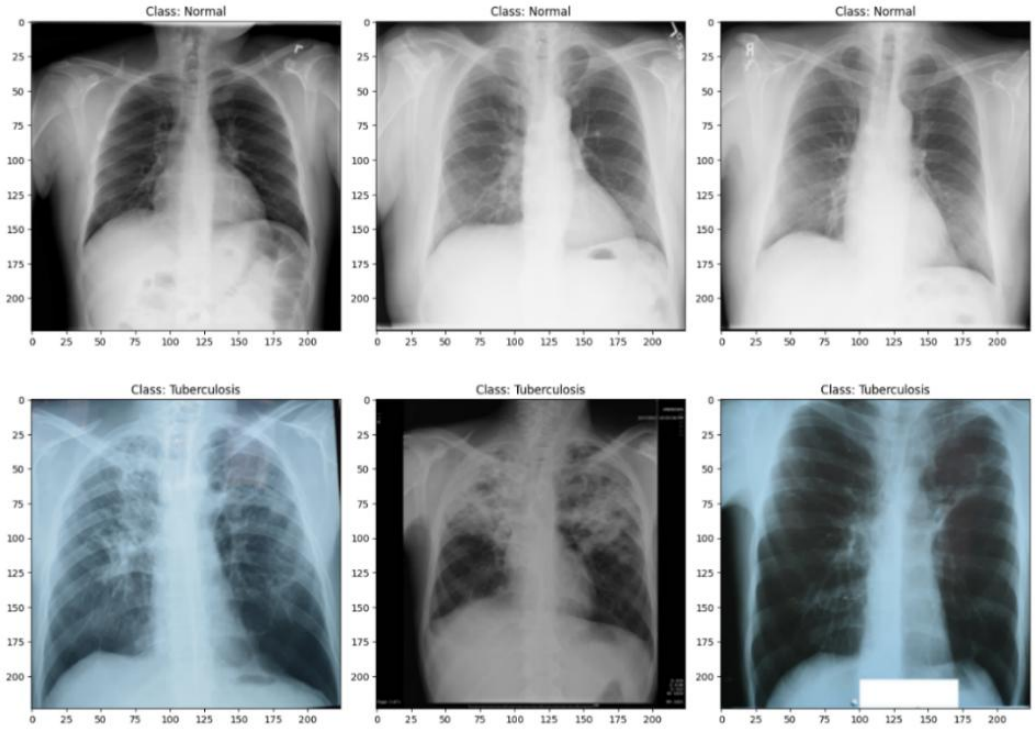

Figure 3. Samples of images per category

Preprocessing

During the preprocessing stage, several steps were taken to convert the raw data into a format suitable for analysis and model training [19]. The process began with dividing the dataset into training, validation, and testing subsets to ensure effective learning and objective evaluation.

First, pixel intensity normalization was applied to scale the values into a defined range, simplifying computation and improving convergence speed during training. The images were then resized to maintain consistent dimensions, ensuring compatibility with the model architecture. Overall, these preprocessing steps aim to optimize data quality and prepare it for subsequent feature extraction and model development.

The initial step involves data splitting, which is crucial for promoting robust model generalization. The dataset is divided into three subsets: 70% for training, 15% for validation, and 15% for testing, following the approach adopted by Vanitha et al. (2025) [20]. The training set is used to construct and optimize the model, while the validation set monitors its performance during training and guides hyperparameter tuning. The testing set, on the other hand, provides an unbiased evaluation of the model's ability to generalize to previously unseen data. This partitioning strategy ensures that the model learns patterns effectively and performs reliably in real-world applications. The distribution of images across these subsets is illustrated in the vertical bar chart shown in Figure 4.

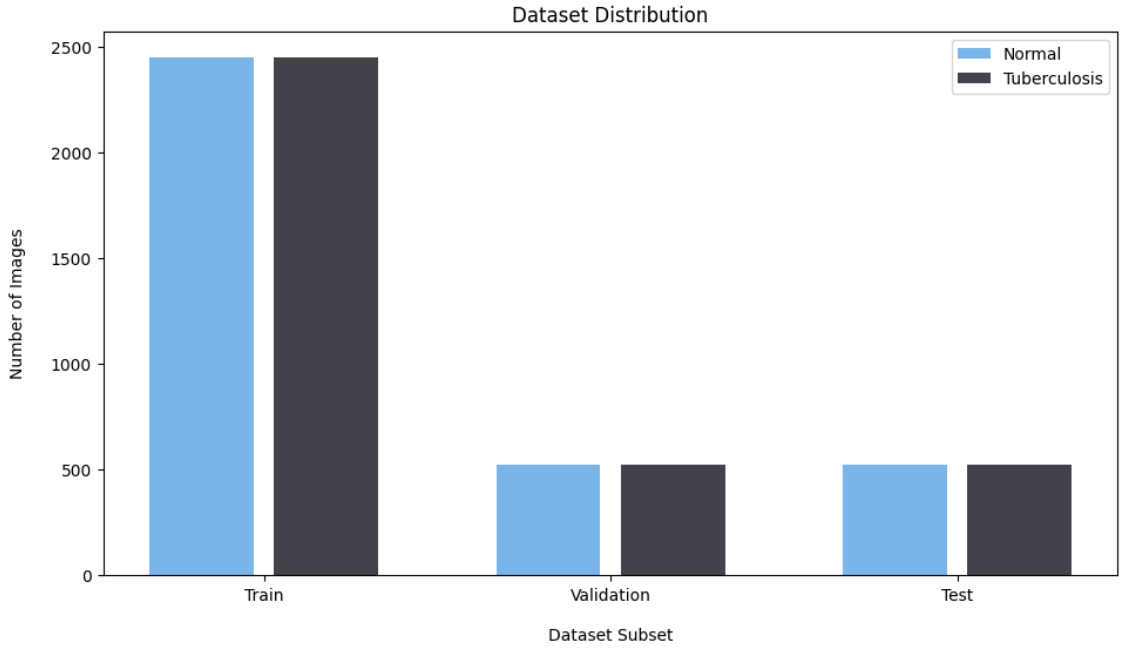

Figure 4. Dataset split distribution

After dividing the dataset, normalization was applied to scale and transform the input data, improving model performance and training stability. This process adjusts feature ranges and distributions to ensure greater statistical consistency, facilitating more effective learning [21]. This study's normalization involved rescaling pixel intensity values from their original range of 0–255 to a normalized range of 0–1 by dividing by 255 [22]. This preprocessing step reduces computational complexity and allows the network to focus on identifying meaningful patterns, minimizing the influence of large-scale variations in pixel values [23]. By normalizing the data before further processing, the model trains more efficiently and achieves higher accuracy in classification tasks.

Following normalization, the next step in preprocessing was image resizing, a fundamental procedure in computer vision tasks [24]. This step ensured that all images had consistent dimensions, which is essential for reliable analysis and maintaining model accuracy [25]. In this study, each image was resized to 224 × 224 pixels to meet the input requirements of DenseNet-169 [26]. Standardizing the image size enhances computational efficiency and preserves dimensional consistency across the dataset. Additionally, resizing allows the model to process images within a uniform pixel space while minimizing the risk of losing important visual details [27]. To maintain consistency, all images in the training, validation, and testing sets were resized using an image generator, enabling the model to detect patterns more effectively and achieve optimal classification performance.

Model Building

In this study, DenseNet-169 was utilized as the backbone model, enhanced by adding a CBAM to help the network concentrate on the most significant features, in line with the methodology of Zhang et al. (2020) [28]. The model processes chest X-ray images in RGB format, sized at 224 × 224 pixels, while preserving the spatial layout for effective pattern recognition. The architecture begins with a 7 × 7 convolution layer that uses a stride of 2 to capture broad spatial information, followed by a 3 × 3 max-pooling layer, which reduces the image size while maintaining key features. At the network's core are four dense blocks, each composed of 1 × 1 and 3 × 3 convolution layers. After each dense block, CBAM is applied to refine the feature maps by emphasizing crucial channels and important spatial regions. Transition layers between dense blocks utilize 1×1 convolution and 2×2 average pooling to downscale feature maps and maintain balanced growth. After the last dense block, global average pooling condenses spatial patterns into a one-dimensional feature vector. This vector is subsequently input into a dense layer with 512 units, activated by ReLU, combined with L2 regularization, batch normalization, and a dropout rate of 30% for effective feature integration. Activated by a

sigmoid, the final output layer delivers a probability value to classify chest X-ray images as normal or tuberculosis. The model's architecture is depicted in Figure 5.

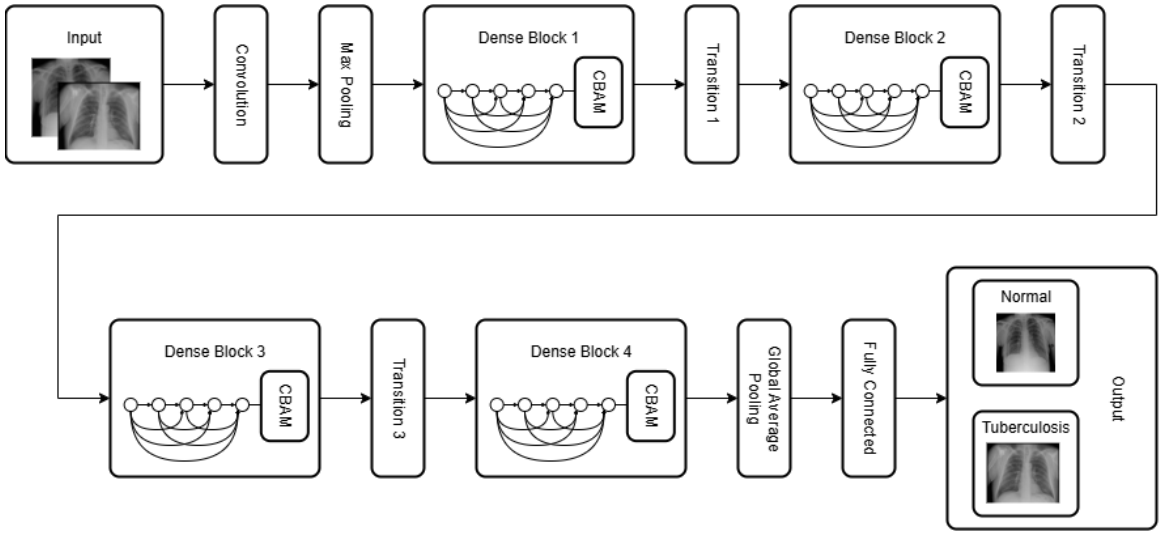

Figure 5. Proposed model architecture

Model Training

Model training in this study was conducted using a deep learning approach involving forward propagation and backpropagation to optimize the neural network weights. The architecture integrates DenseNet-169 as a feature extractor with the CBAM to enhance the model's focus on relevant features. Training was carried out iteratively as chest X-ray images were processed in batches, passing through several transformation stages during forward propagation, followed by weight updates via backpropagation. The process involves six main stages: forward propagation, attention application, global pooling and feature flattening, fully connected layer processing, backpropagation, and weight updating. In the forward pass, input images move through multiple convolutional layers of DenseNet-169 to extract hierarchical features, forming the basis for classification [29]. These features are then refined using CBAM, which applies channel and spatial attention to highlight important visual patterns related to tuberculosis [30]. Global Average Pooling converts spatial dimensions into a single vector for each channel, minimizing overfitting [31], and the features are then flattened to fit into the fully connected layer [32]. A dense layer with 512 units using ReLU activation integrates the features before passing them to a sigmoid-activated output neuron for binary classification. After generating predictions, the model calculates the error using binary cross-entropy loss, which is then propagated backward through the network to adjust the weights accordingly [33], [34]. The Adam optimizer is used to iteratively adjust the weights, minimizing errors over the course of training [35].

Model Evaluation

The performance of the proposed model was evaluated using a set of widely accepted metrics to determine its ability to classify chest X-ray images as either Normal or Tuberculosis. A confusion matrix was utilized to display the counts of true positives (TP), true negatives (TN), false positives (FP), and false negatives (FN), providing a clear overview of the model's classification patterns. Overall performance was measured using accuracy, which is calculated as the proportion of correct predictions out of all predictions [36]:

$$\text{Accuracy} = \frac{\text{TP+TN}}{\text{TP+TN+FP+FN}} \tag{1}$$

Precision assessed the proportion of accurate positive predictions [36], reflecting the model's reliability in identifying tuberculosis cases:

$$\text{Precision} = \frac{\text{TP}}{\text{TP+FP}} \tag{2}$$

Recall, also known as sensitivity, indicates the fraction of actual positive cases correctly detected [36], showcasing the model's ability to capture instances of tuberculosis:

$$\text{Recall} = \frac{\text{TP}}{\text{TP+FN}} \tag{3}$$

To balance precision and recall, especially in cases of class imbalance, the F1-score was computed as their harmonic mean [36]:

$$\text{F1} - \text{Score} = 2 \times \frac{\text{Precision} \times \text{Recall}}{\text{Precision} + \text{Recall}} \tag{4}$$

The structure of the confusion matrix, illustrating the relationship between the actual and predicted classes, is presented in Table 1.

Table 1. Confusion matrix

Confusion Matrix		Predicted Class	
		Positive	Negative
Actual Class	Positive	True Positive	False Negative
	Negative	False Positive	True Negative

3. RESULTS AND DISCUSSIONS

Before evaluating the model's classification performance, the dataset underwent crucial preprocessing steps to ensure optimal data quality and consistency. As established previously, the raw chest X-ray images were successfully standardized to uniform dimensions of 224 × 224 pixels and their pixel intensities were normalized to a 0–1 scale. This procedure effectively reduced computational complexity while enhancing the distinctiveness of critical visual features within the scans. The successful application of these preprocessing techniques yielded a refined and highly consistent dataset, providing a robust and reliable foundation for the subsequent model training phases. A representative sample of this final preprocessed dataset is shown in Figure 6.

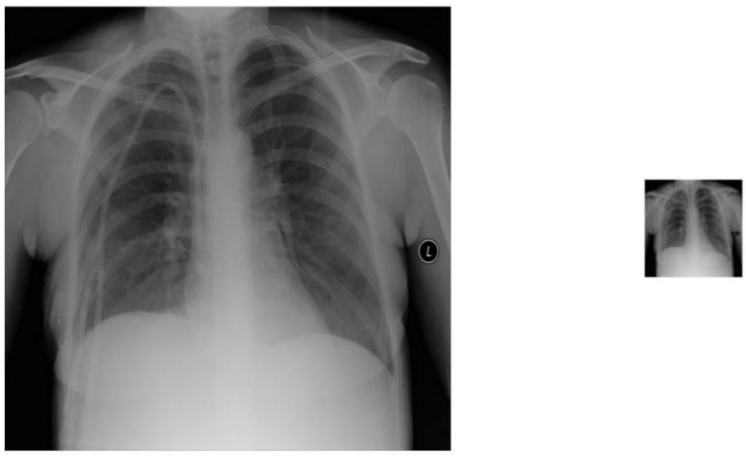

(a) (b)

Figure 6. Image preprocessing results: (a) raw image; (b) preprocessed image

Following the dataset preparation, two experimental scenarios were conducted to evaluate the effectiveness of the DenseNet-169 architecture in classifying the preprocessed chest X-ray images. These experiments were designed to observe the progressive impact of incorporating the Convolutional Block Attention Module (CBAM) into the network. In the first setup, the baseline DenseNet-169 model was initialized with pre-trained weights, leveraging prior knowledge extracted from large-scale datasets. The second setup combined these pre-trained weights with the integrated CBAM module to assess the optimal performance and attention-driven feature extraction of the model. The training outcomes of both experimental setups are illustrated in Figure 7.

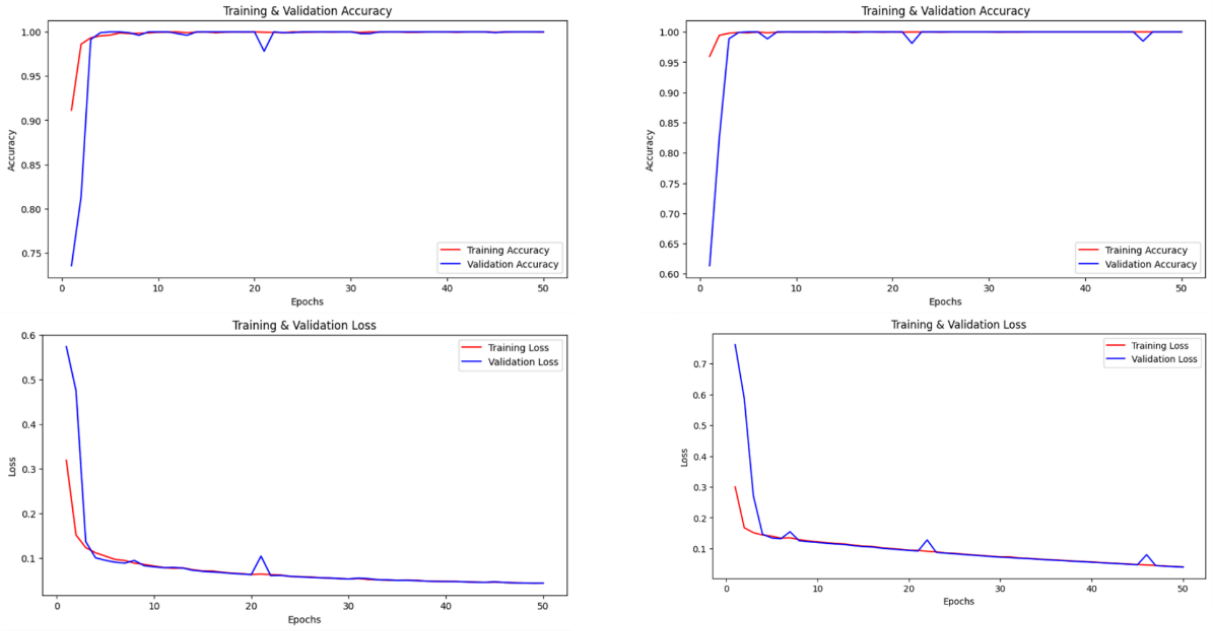

Figure 7. Training result of each scenario

The model was trained for 50 epochs under these two distinct configurations. The pre-trained DenseNet-169 model rapidly increased training and validation accuracy in the first configuration, exceeding 99% by the fourth epoch. However, some variations were noted in the validation results. Consistent and balanced results in the second configuration were observed, which integrated CBAM into the pre-trained DenseNet-169. Both training and validation accuracy quickly surpassed 99%, while loss values steadily decreased, indicating effective feature learning and strong generalization capabilities. Combining DenseNet-169 with the CBAM module provided the most reliable and optimal performance. The effectiveness of each configuration was further evaluated using a confusion matrix, with the corresponding results displayed in Figure 8.

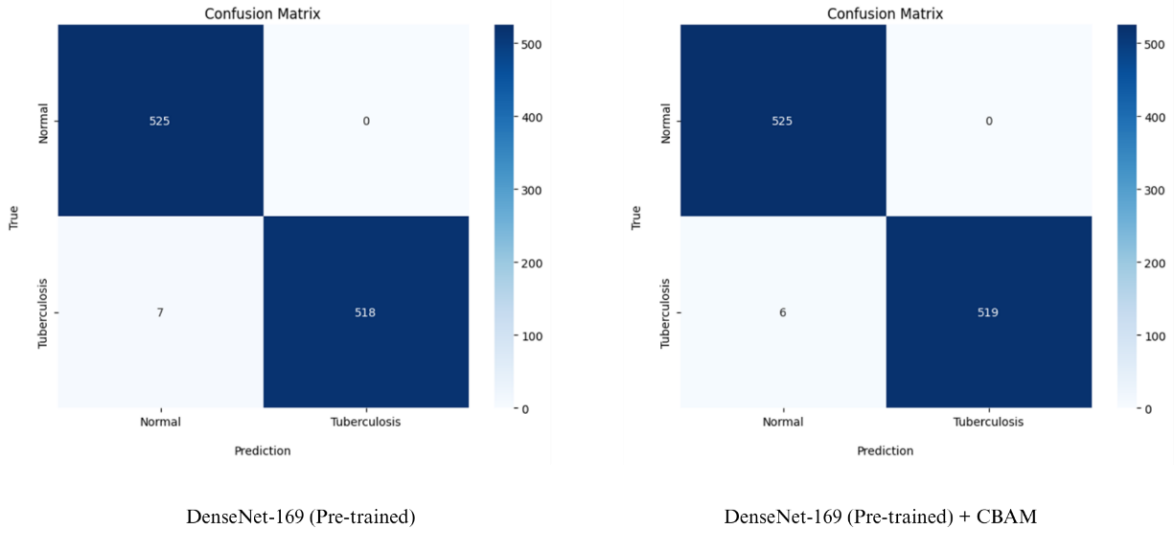

Figure 8. Confusion matrix of each scenario

This study investigates two image classification scenarios to identify the configuration that delivers the best performance, assessed through accuracy, precision, recall, and F1-score metrics. The first experiment involves developing a DenseNet-169 model initialized with pre-trained weights. The second experiment enhances this architecture by incorporating a Convolutional Block Attention Module (CBAM) to improve the network's ability to focus on important image features. Both scenarios are tested using various strategies to mitigate overfitting and enhance overall classification capability. The comparative results of these experiments

are presented in tables and graphs, providing a detailed overview of the effectiveness and efficiency of each approach, as summarized in Table 2.

Table 2. Evaluation result of each scenario

Scenarios	Accuracy	Precision	Recall	F1-Score
DenseNet-169 (Pre-trained)	0,9933	0,9934	0,9933	0,9933
DenseNet-169 (Pre-trained) + CBAM	0,9943	0,9944	0,9943	0,9943

The comparative analysis between the two experimental scenarios demonstrates that the DenseNet-169 model integrated with CBAM achieved superior performance. Incorporating the CBAM module into the DenseNet-169 model with pre-trained weights consistently improved the results, yielding an accuracy of 99.43%, precision of 99.44%, recall of 99.43%, and an F1-score of 99.43%. These outcomes slightly exceeded those of the baseline model from the first scenario, which obtained an accuracy of 99.33%, precision of 99.34%, recall of 99.33%, and an F1-score of 99.33%. Thus, the configuration combining DenseNet-169 with CBAM performed better overall than the baseline approach.

Throughout the 50 training epochs, performance indicators such as training and validation accuracy were monitored to assess stability and generalization. Using a fixed number of epochs helped to evaluate the accuracy gap between the training and validation data, serving as a key measure of potential overfitting. The results of the scenario with DenseNet-169 and CBAM showed a stable alignment between training and validation accuracy. This indicates that the model could maintain classification performance on unseen data while demonstrating stronger generalization compared to the baseline.

Furthermore, a comparative study was conducted against several prior works that utilized the Tuberculosis (TB) Chest X-ray Database but employed alternative deep learning models and methodologies. This comparison aimed to assess the relative effectiveness of the proposed approach in relation to established methods. A summary of the accuracy results from this research, alongside selected previous studies, is presented in Table 3.

Table 3. Comparison with previous studies

Author	Method	Dataset	Result
Rajakumar et al. (2021) [37]	Dual Deep Learning (VGG16 + VGG19) with Mayfly Feature Selection and KNN Classification	Tuberculosis (TB) Chest X-ray Database	97,8%
G. Verma et al. (2023) [38]	Hybrid Model (DenseNet169 + MobileNetV2) with Gabor Filter and Canny Edge Detection	Tuberculosis (TB) Chest X-ray Database	97,9%
Sarawagi et al. (2024) [39]	Self-trained CNN with Wavelet Transform, CLAHE, Gamma Correction, and Data Augmentation	Tuberculosis (TB) Chest X-ray Database	96,57%
Yadav et al. (2024) [40]	CNN with ML Classifiers (SVM, LR, KNN, NB, DT, RF)	Tuberculosis (TB) Chest X-ray Database	95,60%
Maheswari et al. (2024) [41]	Explainable Deep Learning with Shallow-CNN, Bayesian Optimization, and Interpretation with CAM and LIME	Tuberculosis (TB) Chest X-ray Database	95%
Proposed Method	DenseNet-169 and Convolutional Block Attention Module	Tuberculosis (TB) Chest X-ray Database	99,43%

Based on Table 3, the proposed method in this study, which integrates a CNN architecture using DenseNet-169 with the Convolutional Block Attention Module (CBAM), achieved the highest classification accuracy of 99.43% on the Tuberculosis (TB) Chest X-ray Database. This performance surpasses five previous studies utilizing the same dataset. The superior results can be attributed to DenseNet-169's deep feature extraction capability and CBAM's ability to emphasize important spatial and channel features adaptively. This synergy enables the model to focus more effectively on relevant regions within the chest X-ray images, contributing significantly to improved classification accuracy compared to earlier approaches.

4. CONCLUSION

This study successfully developed a binary classification model for detecting tuberculosis in chest X-ray images using transfer learning with the DenseNet-169 architecture. The model's performance was further improved by incorporating the Convolutional Block Attention Module (CBAM), which effectively emphasizes spatial and channel-relevant features. The experimental process included structured preprocessing steps, such

as normalization and image resizing, and involved training on data from the Tuberculosis (TB) Chest X-ray Database. The addition of CBAM resulted in significant enhancements to the model's effectiveness. The best classification results were obtained with the pre-trained DenseNet-169 combined with CBAM, achieving an impressive accuracy of 99.43%, a precision of 99.72%, a recall of 99.14%, and an F1-score of 99.43%. These findings demonstrate that integrating attention mechanisms with transfer learning significantly enhances classification accuracy and improves the ability to capture discriminative features in tuberculosis detection. Despite these promising results, this study acknowledges certain limitations. Primarily, the model is restricted to binary classification and cannot currently distinguish tuberculosis from other thoracic diseases that manifest with similar radiological patterns. Furthermore, while the model demonstrates high internal validity, its performance may vary when exposed to data from different populations or varying X-ray acquisition equipment. For future research, it is recommended to evaluate the proposed model on larger, multi-institutional datasets to further validate its generalizability. Additionally, testing the model in real-world clinical settings could provide deeper insights into its practical utility.

REFERENCES

[1] A. Vernyuy, "Impact of Technological Advancements on Human Existence," 2024.

[2] R. Sinha, "The role and impact of new technologies on healthcare systems," *Discov. Heal. Syst.*, no. July, 2024, doi: 10.1007/s44250-024-00163-w.

[3] S. Aminizadeh *et al.*, "The applications of machine learning techniques in medical data processing based on distributed computing and the Internet of Things," *Comput. Methods Programs Biomed.*, vol. 241, no. July, p. 107745, 2023, doi: 10.1016/j.cmpb.2023.107745.

[4] P. K. Mall *et al.*, "A comprehensive review of deep neural networks for medical image processing: Recent developments and future opportunities," *Healthc. Anal.*, vol. 4, no. April, p. 100216, 2023, doi: 10.1016/j.health.2023.100216.

[5] A. Natarajan, P. M. Beena, A. V. Devnikar, and S. Mali, "A systemic review on tuberculosis," Jul. 2020, *Tuberculosis Association of India*. doi: 10.1016/j.ijtb.2020.02.005.

[6] S. D. Alipoor, I. M. Adcock, P. Tabarsi, G. Folkerts, and E. Mortaz, "MiRNAs in tuberculosis: Their decisive role in the fate of TB," Nov. 2020, *Elsevier B.V.* doi: 10.1016/j.ejphar.2020.173529.

[7] L. Muthukrishnan, "Multidrug resistant tuberculosis – Diagnostic challenges and its conquering by nanotechnology approach – An overview," Mar. 2021, *Elsevier Ireland Ltd*. doi: 10.1016/j.cbi.2021.109397.

[8] M. L. Carabalí-Isajar *et al.*, "Clinical manifestations and immune response to tuberculosis," Aug. 2023, *Springer Science and Business Media B.V.* doi: 10.1007/s11274-023-03636-x.

[9] H. Chen, W. Gu, H. Zhang, Y. Yang, and L. Qian, "Research on improved YOLOv8s model for detecting mycobacterium tuberculosis," *Heliyon*, vol. 10, no. 18, Sep. 2024, doi: 10.1016/j.heliyon.2024.e38088.

[10] W. H. Organization, *Global Tuberculosis Report 2024*. Geneva: World Health Organization, 2024.

[11] V. Singh, "Tuberculosis treatment-shortening," May 2024, *Elsevier Ltd*. doi: 10.1016/j.drudis.2024.103955.

[12] A. Celeghin *et al.*, "Convolutional neural networks for vision neuroscience: significance, developments, and outstanding issues," 2023, *Frontiers Media SA*. doi: 10.3389/fncom.2023.1153572.

[13] X. Zhao, L. Wang, Y. Zhang, X. Han, M. Deveci, and M. Parmar, "A review of convolutional neural networks in computer vision," *Artif. Intell. Rev.*, vol. 57, no. 4, Apr. 2024, doi: 10.1007/s10462-024-10721-6.

[14] I. H. Sarker, "Deep Learning: A Comprehensive Overview on Techniques, Taxonomy, Applications and Research Directions," Nov. 2021, *Springer*. doi: 10.1007/s42979-021-00815-1.

[15] M. B. Mizan, M. A. M. Hasan, and S. R. Hassan, "A comparative study of tuberculosis detection using deep convolutional neural network," in *2020 2nd International Conference on Advanced Information and Communication Technology, ICAICT 2020*, Institute of Electrical and Electronics Engineers Inc., Nov. 2020, pp. 157–161. doi: 10.1109/ICAICT51780.2020.9333464.

[16] Y. Liu, F. Liu, S. Tu, S. Liu, and B. Han, "Attention enhanced residual network for automatic pulmonary tuberculosis detection on chest radiographs images," *Digit. Signal Process. A Rev. J.*, vol. 159, Apr. 2025, doi: 10.1016/j.dsp.2024.104975.

[17] T. Rahman *et al.*, "Reliable tuberculosis detection using chest X-ray with deep learning, segmentation and visualization," *IEEE Access*, vol. 8, pp. 191586–191601, 2020, doi: 10.1109/ACCESS.2020.3031384.

[18] T. Rahman, A. Khandakar, and M. E. H. Chowdhury, "Tuberculosis (TB) Chest X-ray Database," 2020, *IEEE DataPort*.

[19] I. D. Acheme and O. R. Vincent, "Machine-learning models for predicting survivability in COVID-19 patients," in *Data Science for COVID-19 Volume 1: Computational Perspectives*, Elsevier, 2021, pp. 317–336. doi: 10.1016/B978-0-12-824536-1.00011-3.

[20] K. Vanitha, T. R. Mahesh, V. V. Kumar, and S. Guluwadi, "Enhanced tuberculosis detection using Vision Transformers and explainable AI with a Grad-CAM approach on chest X-rays," *BMC Med. Imaging*, vol. 25, no. 1, Dec. 2025, doi: 10.1186/s12880-025-01630-3.

[21] G. Habib, A. Malik, and J. Ahmad, "Exploring the Efficacy of Group-Normalization in Deep Learning Models for Alzheimer's Disease Classification," 2024.

[22] X. Pei *et al.*, "Robustness of machine learning to color, size change, normalization, and image enhancement on micrograph datasets with large sample differences," *Mater. Des.*, vol. 232, p. 112086, Aug. 2023, doi: 10.1016/j.matdes.2023.112086.

[23] L. Huang, J. Qin, Y. Zhou, F. Zhu, L. Liu, and L. Shao, "Normalization Techniques in Training DNNs: Methodology, Analysis and Application," *IEEE Trans. Pattern Anal. Mach. Intell.*, vol. 45, no. 8, pp. 10173–10196, 2023, doi: 10.1109/TPAMI.2023.3250241.

[24] S. Saponara and A. Elhanashi, "Impact of Image Resizing on Deep Learning Detectors for Training Time and Model Performance," in *Lecture Notes in Electrical Engineering*, Springer Science and Business Media Deutschland GmbH, 2022, pp. 10–17. doi: 10.1007/978-3-030-95498-7_2.

[25] N. Saurina, N. Chamidah, R. Rulaningtyas, and A. Aryati, "Classification and Counting of Mycobacterium Tuberculosis using YOLOv5," *J. Inf. Syst. Eng. Bus. Intell.*, vol. 11, no. 2, pp. 267–278, Jun. 2025, doi: 10.20473/jisebi.11.2.267-278.

[26] S. Katreddi, A. Midatani, A. P. Roy, U. Velpuri, and S. Kasani, "Pediatric pneumonia X-ray image classification: predictive model development with DenseNet-169 transfer learning," *J. Med. Artif. Intell.*, vol. 8, Dec. 2025, doi: 10.21037/jmai-24-356.

[27] M. E. Rayed, S. M. S. Islam, S. I. Niha, J. R. Jim, M. M. Kabir, and M. F. Mridha, "Deep learning for medical image segmentation: State-of-the-art advancements and challenges," Jan. 2024, *Elsevier Ltd*. doi: 10.1016/j.imu.2024.101504.

[28] Y. Zhang, M. Xu, and X. Li, "Remote Sensing Image Retrieval Based on DenseNet Model and CBAM," in *2020 IEEE 3rd*

International Conference on Computer and Communication Engineering Technology (CCET), 2020, pp. 86–90. doi: 10.1109/CCET50901.2020.9213121.

[29] Y. M. Ren *et al.*, "A tutorial review of neural network modeling approaches for model predictive control," Sep. 2022, *Elsevier Ltd*. doi: 10.1016/j.compchemeng.2022.107956.

[30] I. Tahyudin *et al.*, "High-Accuracy Stroke Detection System Using a CBAM-ResNet18 Deep Learning Model on Brain CT Images," *J. Appl. Data Sci.*, vol. 6, no. 1, pp. 788–799, Jan. 2025, doi: 10.47738/jads.v6i1.569.

[31] Z. Tao, C. Xiaoyu, L. Huiling, Y. Xinyu, L. Yuncan, and Z. Xiaomin, "Pooling Operations in Deep Learning: From 'Invariable' to 'Variable,'" 2022, *Hindawi Limited*. doi: 10.1155/2022/4067581.

[32] R. Ghosh, "Determining Top Fully Connected Layer's Hidden Neuron Count for Transfer Learning, Using Knowledge Distillation: a Case Study on Chest X-Ray Classification of Pneumonia and COVID-19," *J. Digit. Imaging*, vol. 34, no. 6, pp. 1349–1358, Dec. 2021, doi: 10.1007/s10278-021-00518-2.

[33] J. Terven, D. M. Cordova-Esparza, A. Ramirez-Pedraza, E. A. Chavez-Urbiola, and J. A. Romero-Gonzalez, "Loss Functions and Metrics in Deep Learning," Apr. 2025, doi: 10.1007/s10462-025-11198-7.

[34] S. Amin, "Backpropagation – Artificial Neural Network (BP-ANN): Understanding gender characteristics of older driver accidents in West Midlands of United Kingdom," *Saf. Sci.*, vol. 122, Feb. 2020, doi: 10.1016/j.ssci.2019.104539.

[35] E. Hassan, M. Y. Shams, N. A. Hikal, and S. Elmougy, "The effect of choosing optimizer algorithms to improve computer vision tasks: a comparative study," *Multimed. Tools Appl.*, vol. 82, no. 11, pp. 16591–16633, May 2023, doi: 10.1007/s11042-022-13820-0.

[36] V. T. Q. Huy and C. M. Lin, "An Improved Densenet Deep Neural Network Model for Tuberculosis Detection Using Chest X-Ray Images," *IEEE Access*, vol. 11, pp. 42839–42849, 2023, doi: 10.1109/ACCESS.2023.3270774.

[37] M. P. Rajakumar, R. Sonia, B. Uma Maheswari, and S. P. Karuppiah, "Tuberculosis detection in chest X-ray using Mayfly-algorithm optimized dual-deep-learning features," *J. Xray. Sci. Technol.*, vol. 29, no. 6, pp. 961–974, 2021, doi: 10.3233/XST-210976.

[38] G. Verma, A. Kumar, and S. Dixit, "Early detection of tuberculosis using hybrid feature descriptors and deep learning network," *Polish J. Radiol.*, vol. 88, no. 1, pp. e445–e454, 2023, doi: 10.5114/pjr.2023.131732.

[39] K. Sarawagi, A. Pagrotra, H. Dhiman, and N. Singh, "Self-Trained Convolutional Neural Network (CNN) for Tuberculosis Diagnosis in Medical Imaging," *Cureus*, Jun. 2024, doi: 10.7759/cureus.63356.

[40] S. Yadav, S. A. M. Rizvi, and P. Agarwal, "Detection of Lung Diseases for Pneumonia, Tuberculosis, and COVID-19 with Artificial Intelligence Tools," *SN Comput. Sci.*, vol. 5, no. 3, Mar. 2024, doi: 10.1007/s42979-024-02617-7.

[41] B. U. Maheswari *et al.*, "Explainable deep-neural-network supported scheme for tuberculosis detection from chest radiographs," *BMC Med. Imaging*, vol. 24, no. 1, Dec. 2024, doi: 10.1186/s12880-024-01202-x.

.